THE ASTROPHYSICAL JOURNAL, 398:394–406, 1992 October 10

IRON IONIZATION AND RECOMBINATION RATES AND IONIZATION EQUILIBRIUM

M. ARNAUD[1] AND J. RAYMOND
Harvard-Smithsonian Center for Astrophysics, 60 Garden Street, Cambridge, MA 02138
Received 1992 January 2; accepted 1992 April 20

ABSTRACT

In the past few years important progress has been made on the knowledge of ionization and recombination rates of iron, an astrophysically abundant heavy element and a major impurity in laboratory fusion devices. Detailed calculations of ionization cross sections (direct and excitation autoionization process) and dielectronic recombination rate coefficients have now been performed for the whole iron isonuclear sequence. Crossed beam measurements of ionization cross sections are available for some iron ions. We make a critical review of the existing data on ionization and dielectronic recombination and present new computations of radiative recombination rate coefficients of Fe^{+14} through Fe^{+25} using the photoionization cross sections of Clark et al. We provide analytical fits to the recommended data (direct ionization and excitation-autoionization cross sections; radiative and dielectronic recombination rate coefficients). Finally we determine the iron ionic fractions at ionization equilibrium and compare them with previous computations as well as with observational data.

Subject headings: atomic data — atomic processes

1. INTRODUCTION

Knowledge of electron impact ionization and recombination rates is essential for the analysis of laboratory and astrophysical plasmas. Of special interest are the rates for iron which is an astrophysically abundant element and a major impurity in laboratory fusion devices.

Due to the difficulty of producing multicharged metal ions, crossed beam measurements of iron ionization cross sections became available only recently (Montague, Diserens, & Harrison 1984; Mueller et al. 1985; Gregory et al. 1986, 1987). Theoretical computations too, for both direct (DI) and excitation autoionization (EA) process, have now been performed for the whole iron isonuclear sequence (Younger 1981a, 1982, 1983a; Pindzola, Griffin, & Bottcher 1986; Butler & Moores 1985; Griffin, Pindzola, & Bottcher 1987; Pindzola et al. 1987). All these data were extensively reviewed by Pindzola et al. (1987, hereafter PGBYH), who also proposed formulae fitting the total ionization rate coefficients (derived either from measured cross sections or theory). In view of these new results we thought it worthwhile to update the ionization rate coefficients proposed by Arnaud & Rothenflug (1985, hereafter Paper I), using as guidelines the prescriptions of PGBYH. However a major difference from their work is that, following the philosophy of Paper I, we prefer to propose parametric formulae reproducing the DI (from each shell) and EA *cross sections* separately, from which the rate coefficients can be deduced readily. Indeed the adoption of such formulae, which are based on the cross section behavior expected from theoretical computations, permits a more physically meaningful fit to the measurements, as well as to ensure a correct behavior at high energies (where experimental data are usually missing), and easier discussion of the behavior of the ionization cross sections along isoelectronic sequences (see Paper I). Moreover it is easy to fit the cross sections in a form, easy to integrate over a Maxwellian distribution, which gives a correct behavior near threshold. Thus this method gives accurate rate coefficients at very low temperatures, where they increase very rapidly and cannot be accurately fitted with the Chebychev polynomials adopted by PGBYH.

Dielectronic recombination dominates the recombination rates of many ions in hot plasmas. The Burgess (1965) General Formula have been widely used to compute the dielectronic recombination rate coefficients (e.g., Woods, Shull, & Sarazin 1981 calculations for low charge iron ions). Jacobs et al. (1977) pointed out the importance of autoionization into excited states of the recombining ion, a process not taken into account in the General Formula. This process can reduce drastically the recombination rate. The Jacobs et al. calculations (Fe^{+8}–Fe^{+25}) tend, however, to overestimate the effect for highly charged ions (see below). In Paper I we used the computations of Woods et al. and Jacobs et al., except for H- and He-like ions for which more detailed computations were available. There are now detailed calculations for most iron ions. We review these new computations and fit the adopted rate coefficients with analytic formulae. Finally the radiative recombination rate coefficients can be deduced from the photoionization cross sections using the Milne relation of detailed balance. We reestimated the recombination rate coefficients of Fe^{+14} through Fe^{+25} using the photoionization cross sections of Clark, Cowan, & Bobrowicz (1986) who made the first computations of partial photoionization cross sections for excited levels in He-like through Al-like isoelectronic sequences.

Section 2 deals with ionization rates, §§ 3 and 4 with radiative and dielectronic recombination rates, respectively. Finally in § 5 we present and discuss the ionization equilibria obtained in the framework of this study.

[1] On leave from Service d'Astrophysique, CEN Saclay, 91191 Gif sur Yvette Cedex, France (Postal address).

2. IONIZATION RATES

For the direct ionization cross sections we use the same parametric formula as in Paper I, originally proposed by Younger (1981a) and adopted by PGBYH for the theoretical cross sections:

$$\sigma_{DI}(E) = \sum_j \frac{1.}{u_j I_j^2}\left[A_j\left(1-\frac{1}{u_j}\right) + B_j\left(1-\frac{1}{u_j}\right)^2 + C_j Ln(u_j) + D_j\frac{Ln(u_j)}{u_j}\right] \text{cm}^2 \text{ with } u_j = \frac{E}{I_j}. \quad (1)$$

TABLE 1

A. DIRECT IONIZATION COEFFICIENTS

Ion	Shell	Potential (eV)	A	B	C (10^{-14} cm^2 eV^2)	D	Reference	Note
Fe^{+0}	$4s^2$	7.9	31.9	−15.0	0.32	−28.1	(1)	a
	$3d^6$	9.0	15.0	−16.7	7.00	−12.7		
	$3p^6$	59.0	115.	−72.4	9.57	−107.		
Fe^{+1}	4s	16.18	17.4	−3.27	0.16	−10.2	(2)	
	$3d^6$	24.83	30.1	−38.8	18.6	−45.7		
	$3p^6$	83.37	115.	−72.4	9.57	−107.		
Fe^{+2}	$3d^6$	34.75	84.8	−67.6	21.0	−84.1	(3)	b
	$3p^6$	93.28	87.7.	−49.6	16.4	−84.8		
	$3s^2$	131.9	25.9	−11.7	2.32	−23.9		
Fe^{+3}	$3d^5$	53.74	77.4	−43.9	19.6	−81.9	(4)	
	$3p^6$	111.9	79.1	−30.0	8.38	−74.6		
	$3s^2$	151.0	16.7	−3.44	2.32	−15.1		
Fe^{+4}	$3d^4$	75.15	48.1	−20.4	16.2	−48.4	(4)	
	$3p^6$	132.7	66.8	−18.9	9.29	−60.5		
	$3s^2$	172.4	13.4	−0.410	2.33	−10.9		
Fe^{+5}	$3d^3$	98.69	36.9	−11.8	10.3	−31.5	(5)	
	$3p^6$	155.5	67.0	−18.6	9.43	−56.5		
	$3s^2$	195.8	12.7	−0.086	2.42	−8.97		
Fe^{+6}	$3d^2$	124.2	14.6	−4.36	5.98	−10.5	(5)	
	$3p^6$	180.0	67.9	−20.6	9.82	−53.7		
	$3s^2$	220.9	15.6	−2.29	2.3	−10.6		
Fe^{+7}	3d	151.7	14.3	−4.44	2.45	−9.53	(4)	
	$3p^6$	213.0	69.9	−23.7	9.5	−51.7		
	$3s^2$	249.0	19.2	−5.7	2.3	−12.7		
Fe^{+8}	$3p^6$	235.0	69.9	−23.7	9.5	−51.7	(6)	
	$3s^2$	271.0	19.2	−5.7	2.3	−12.7		
Fe^{+9}	$3p^5$	262.0	57.7	−18.6	7.8	−40.3	(6)	
	$3s^2$	297.0	21.0	−7.1	2.3	−14.1		
Fe^{+10}	$3p^4$	290.0	45.6	−13.9	6.2	−30.0	(6)	
	$3s^2$	324.0	22.8	−8.4	2.3	−15.4		
Fe^{+11}	$3p^3$	331.0	39.2	−9.7	4.4	−20.8	(7)	
	$3s^2$	356.0	24.6	−9.8	2.3	−16.8		
Fe^{+12}	$3p^2$	361.0	21.3	−5.9	3.0	−12.6	(6)	
	$3s^2$	388.0	26.4	−11.2	2.3	−18.1		
Fe^{+13}	3p	392.0	9.1	−2.6	1.4	−5.6	(6, 7)	
	$3s^2$	421.0	28.2	−12.5	2.3	−19.4		
Fe^{+14}	$3s^2$	457.0	19.8	−5.7	2.1	−11.9	(6)	c
	$2p^6$	1185.0	78.9	−27.0	10.6	−52.8		
	$2s^2$	1254.3	23.5	−7.8	3.3	−16.5		
Fe^{+15}	3s	490.0	9.0	−2.6	1.0	−5.4	(7, 8)	
	$2p^6$	1223.0	78.9	−27.0	10.6	−52.8		
	$2s^2$	1298.6	23.5	−7.8	3.3	−16.5		
Fe^{+16}	$2p^6$	1265.0	82.2	−26.4	6.1	−49.8	(9)	
	$2s^2$	1397.0	19.2	−5.5	2.8	−12.3		
Fe^{+17}	$2p^5$	1358.0	68.5	−22.0	5.1	−41.5	(9)	
	$2s^2$	1471.0	19.2	−5.5	2.8	−12.3		
Fe^{+18}	$2p^4$	1456.0	54.8	−17.6	4.1	−33.2	(9)	
	$2s^2$	1548.0	19.2	−5.5	2.8	−12.3		
Fe^{+19}	$2p^3$	1582.0	41.1	−13.2	3.1	−24.9	(9)	
	$2s^2$	1622.0	19.2	−5.5	2.8	−12.3		
Fe^{+20}	$2p^2$	1689.0	27.4	−8.8	2.0	−16.6	(9)	
	$2s^2$	1731.0	19.2	−5.5	2.8	−12.3		
Fe^{+21}	2p	1799.0	13.7	−4.4	1.0	−8.3	(9)	
	$2s^2$	1842.0	19.2	−5.5	2.8	−12.3		
Fe^{+22}	$2s^2$	1950.0	19.2	−5.3	2.7	−12.3	(9)	
	$1s^2$	8482.0	24.1	−7.9	4.1	−18.0		
Fe^{+23}	2s	2045.0	9.3	−2.6	1.4	−5.8	(9)	
	$1s^2$	8580.0	24.1	−7.9	4.1	−18.0		
Fe^{+24}	$1s^2$	8828.0	24.8	−8.4	3.8	−20.0	(9)	
Fe^{+25}	1s	9278.0	13.0	−4.5	1.9	−10.6	(9)	

TABLE 1—*Continued*

B. EXCITATION AUTOIONIZATION COEFFICIENTS[d]

Ion	Potential (eV)	A	B	C (10^{-16} cm^2 eV)	D	E	Reference
Fe^{+0}	0	0	0	0	0	0	
Fe^{+1}	0	0	0	0	0	0	
Fe^{+2}	57.3	8.78 (−1)	0	−1.15 (2)	7.12 (1)	4.79 (1)	(3)
Fe^{+3}	60.	3.02 (0)	6.75 (1)	−5.98 (1)	4.60 (1)	0	(4)
Fe^{+4}	81.	0	2.80 (−1)	−1.62 (1)	3.55 (1)	0	(4)
Fe^{+5}	95.	0	0	−5.83 (0)	1.23 (1)	8.85 (0)	(5)
Fe^{+6}	125.	0	0	−4.81 (1)	4.25 (1)	1.63 (1)	(5)
Fe^{+7}	160.	5.00 (0)	4.30 (1)	−7.26 (1)	4.29 (1)	0	(4)
Fe^{+8}	650.	0	0	0	1.87 (0)	0	(4)
Fe^{+9}	650.	0	0	0	1.96 (0)	0	(4)
Fe^{+10}	650.	0	0	0	3.21 (0)	0	(4)
Fe^{+11}	650.	0	0	0	3.89 (0)	0	(7)
Fe^{+12}	670.	0	0	0	4.10 (0)	0	(4)
Fe^{+13}	671.	0	0	0	5.92 (0)	0	(7, 10)
Fe^{+14}	700.	0	0	0	4.81 (0)	0	(4)
Fe^{+15}	704.	0	0	0	2.95 (0)	0	(4, 11, 12)
Fe^{+16}	0	0	0	0	0	0	
Fe^{+17}	0	0	0	0	0	0	
Fe^{+18}	0	0	0	0	0	0	
Fe^{+19}	0	0	0	0	0	0	
Fe^{+20}	0	0	0	0	0	0	
Fe^{+21}	0	0	0	0	0	0	
Fe^{+22}	0	0	0	0	0	0	
Fe^{+23}	6592.	1.64 (−2)	1.76 (−3)	−1.17 (−2)	0	2.16 (−2)	(13)
Fe^{+24}	0	0	0	0	0	0	
Fe^{+25}	0	0	0	0	0	0	

[a] There was an error in Arnaud & Rothenflug 1985 for this ion. The parameters now listed correspond to the computations of McGuire 1977.

[b] Ionization from the $3p^6$ shell leads to double ionization.

[c] Arnaud & Rothenflug (1985) slightly corrected the A, B, C, D parameters given by Younger 1983a (Table 1) since they give cross sections too high by 10%–20% as compared to the cross sections plotted in his Fig. 3.

[d] 8.78(−1) denotes 8.78×10^{-1}.

REFERENCES.—(1) McGuire 1977, theory; (2) Montague et al. 1984, measurements; (3) Mueller et al. 1985, measurements; (4) PGBYH, theory; (5) Gregory et al. 1986, measurements; (6) Younger (1983a), theory; (7) Gregory et al. 1987 measurements; (8) Younger 1981a, theory; (9) Younger (1982), theory; (10) Golden et al. 1981, theory; (11) Sampson (1982), theory; (12) Griffin et al. 1987, theory; (13) Sampson & Golden 1981 theory.

The summation is performed over the subshells j of the ionizing ion. E is the incident electron energy (in eV), I_j is the ionization potential for the level j (in eV). The parameters A_j, B_j, C_j and D_j are given in Table 1A (in units of 10^{-14} cm^2 eV^2) together with the values of I_j.

The direct ionization rate coefficients versus temperature T are then, where kT and I_j are in eV

$$C_{\rm DI}(T) = \frac{6.69 \times 10^7}{(kT)^{3/2}} \sum_j \frac{\exp(-x_j)}{x_i} F(x_j) \text{ cm}^3 \text{ s}^{-1}$$

$$F(x) = A_j[1 - x_j f_1(x_j)] + B_j[1 + x_j - x_j(2 + x_j) f_1(x_j)] + C_j f_1(x_j) + D_j x_j f_2(x_j) \quad (2)$$

with

$$x_j = \frac{I_j}{kT}; \quad f_1(x) = e^x \int_1^\infty \frac{dt}{t} e^{-tx}; \quad \text{and} \quad f_2(x) = e^x \int_1^\infty \frac{dt}{t} e^{-tx} \text{Ln}(t).$$

For the excitation autoionization process we adopt the following formula for the cross section:

$$\sigma_{\rm EA}(u) = \frac{1.}{uI_{\rm EA}} \left[A + B\left(1 - \frac{1}{u}\right) + C\left(1 - \frac{1}{u^2}\right) + D\left(1 - \frac{1}{u^3}\right) + E \text{Ln}(u) \right] \text{cm}^2 \text{ with } u = \frac{E}{I_{\rm EA}}, \quad (3)$$

where $I_{\rm EA}$ is the excitation autoionization threshold (in eV), E is the incident electron energy (in eV) and A, B, C, D, E are parameters given in Table 1B (in units of 10^{-16} cm^2 eV). This formula is a generalization of the formulae used in Paper I and is similar to the empirical formula used for excitation cross sections (e.g., Mewe 1972). Moreover it is readily integrable (over a Maxwellian distribution for the electrons) in terms of the exponential integral so that the determination of the parameters A, B, C, D, E allows to obtain the rate coefficients directly. The E-A process actually involve many possible excited levels (and threshold), usually resulting in a complex shape of the cross section near the EA onset. Therefore $I_{\rm EA}$ must be considered as an empirical parameter chosen (around the mean excitation energy) so as to fit the data at best.

The EA ionization rate coefficients versus the temperature T is then, where kT and I_{EA} are in eV

$$C_{EA}(T) = \frac{6.69 \times 10^7 \exp(-x)}{\sqrt{kT}} F(x) \text{ cm}^3 \text{ s}^{-1}$$

$$F(x) = A + B[1 - xf_1(x)] + C[1 - x(1 - xf_1(x))] + D\{1 - 0.5[x - x^2 + x^3 f_1(x)]\} + Ef_1(x) \quad (4)$$

with

$$x = \frac{I_{EA}}{kT} \quad \text{and} \quad f_1(x) = e^x \int_1^\infty \frac{dt}{t} e^{-tx}.$$

The results presented below concern ionization of ions in ground state (in opposition to PGBYH who recommended in some cases to use rate coefficients corresponding to excited states). Indeed for low-density astrophysical plasmas (as found in supernova remnants or clusters of galaxies) the lifetime of excited states (even of metastable ones) is always small as compared to the mean collision time. This may not be true for higher density plasmas (such as in the solar corona) but in that case a detailed estimate, for each specific case, must be done. Indeed the relative number of ions, which are ionizing, in each configuration (ground state and excited states) are a priori different from those found in crossed beam experiments. When the parameters recommended here are different from the ones listed in Paper I the corresponding ion is typed in bold face in Table 1A and 1B.

Fe^+ (*configuration* $3p^6 3d^6 4s$).—There is no apparent contribution of the EA process in the measurements of Montague et al. (1984). Though there is some evidence of the presence of excited ions in the beam (metastable state ^4D), Montague et al. (1984) argue that they should not have much influence on the cross sections above 30 eV. The theoretical computations of PGBYH for the DI process (using the average configuration distorted wave method) exceeds the data by about 20%. In view of these new computations we refitted the data, using as guidelines the DI estimates of PGBYH. We first determine the parameters A, B, and D for the $4s$ shells by fitting the data below the onset (25 eV) of the $3d$ shell ionization potential to the value corresponding to ionization from ground state (^6D states, $I = 16.18$ eV, Montague et al. 1984). The parameters for the $3d$ shell were then determined from the rest of the data, keeping the $3p$ parameters of PGBYH. An excellent agreement with the measurement is reached (see Fig.1).

Fe^{+2} *to* Fe^{+7} (*configuration* $3s^2 3p^6 3d^n$).—The EA contribution is very important for these ions, its relative importance increasing as n, the number of electrons in the $3d$ shell, decreases. Measurements exist now for Fe^{+2} (Mueller et al. 1985), Fe^{+5} and Fe^{+6} (Gregory et al. 1986). The recent theoretical computations are in reasonable agreement with these data (Pindzola et al. 1986; PGBYH).

For Fe^{+2}, contribution of ionization from metastable states is clearly apparent in the measurements near the ionization threshold of the $3d$ shell ($I_{3d} = 34.75$ eV). The theoretical computations of PGBYH overestimate the cross sections by about 25%. Therefore we slightly adjusted the parameters A and D for the DI from $3d$ shell by fitting the data in the energy range between ~41 eV (to minimize the contamination from metastable states) and the EA onset. For the $3s^2$ direct ionization we kept the theoretical computations of PGBYH and did not take into account, to fit the data, ionization from the $3p^6$ shell which actually gives rise to

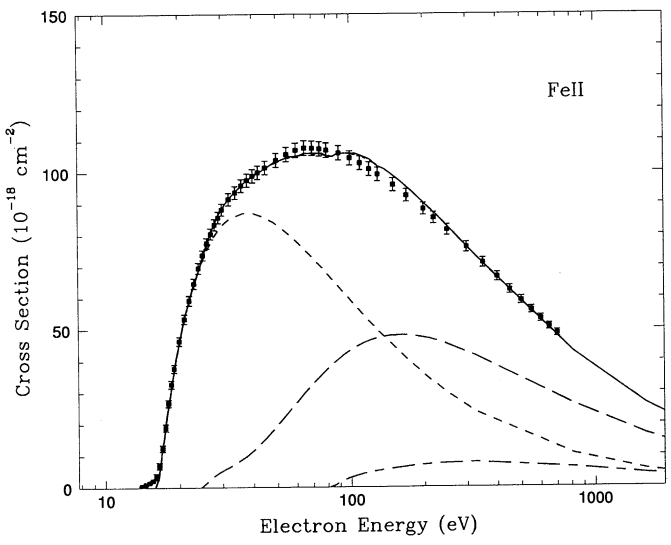

FIG. 1

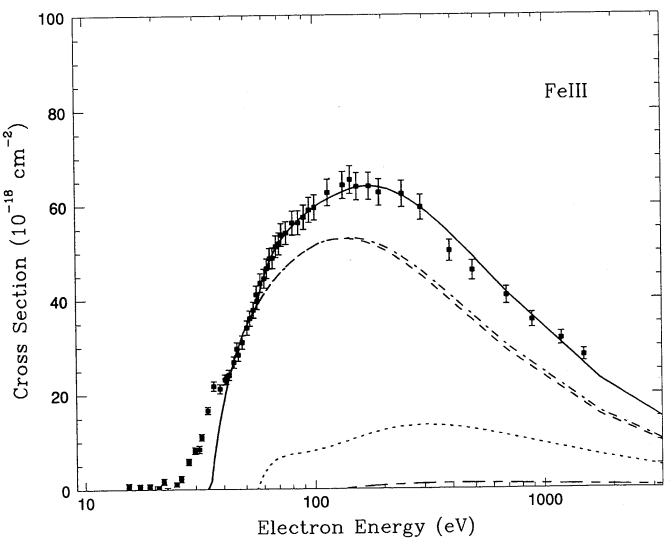

FIG. 2

FIG. 1.—Electron impact ionization cross sections of Fe^{+1} vs. electron energy. *Squares with error bars*: experimental data from Montague et al. (1984). The full curve is the proposed total cross section (best fit to the data with eqs. [1] and [3], the parameters are given in Tables 1A and 1B). *Short dashed curve*: contribution of direct ionization from $4s$ subshell. *Long dashed curve*: contribution of direct ionization from $3d$ subshell. *Long-short dashed curve*: contribution of direct ionization from $3p$ subshell.

FIG. 2.—Same as Fig. 1 for Fe^{+2}. Data points are from Mueller et al. (1985). *Dotted curve*: contribution of excitation autoionization. *Dot-dashed curve*: contribution of total direct ionization. *Short dashed curve*: contribution of direct ionization from $3d$ subshell. *Long-short dashed curve*: contribution of direct ionization from $3s$ subshell.

double ionization[2] (PGBYH). Once the DI was thus estimated we derived the EA contribution by fitting the data above the EA onset. An excellent agreement with the data is reached (see Fig. 2). For Fe^{+5} and Fe^{+6} the EA onset is too close to the 3*d* ionization potential to allow a separate estimate of the DI. Therefore we kept the DI parameters of Pindzola et al. (1986) and only adjusted the EA parameters. The best fits to the data are plotted on Figure 3 (Fe^{+5}) and Figure 4 (Fe^{+6}). For other ions we adopted the theoretical computations of PGBYH. The EA contribution was approximated by formula (3) with less than $\sim 10\%$ error.

The rate coefficients obtained are very different from those obtained from Paper I (discrepancy greater than a factor of 2). This is due to the inclusion of the important EA contribution for all the ions and to more accurate computations of the DI contribution. For instance the ionization rate coefficients are 3.5–4.8 higher for Fe^{+5}–Fe^{+7} at the temperature for which these ions have their maximum abundance, as compared to the rate coefficients given in Paper I, where we did not include any EA contribution by lack of available data.

Fe^{+8} *to* Fe^{+14} (*configuration* $3s^23p^n$).—Measurements exist now for Fe^{+9} (Gregory et al. 1986), Fe^{+11}, and Fe^{+13} (Gregory et al. 1987). In Paper I we estimated the EA cross sections from the scaled hydrogenic collisions strengths computed with the Coulomb-Born-Oppenheimer method in the limit $Z \to \infty$ (Golden et al. 1981). The new computations of Pindzola et al. (1986) and PGBYH made for this purpose in the distorted wave approximation are expected to be more accurate.

The DI contribution parameters are the same as in Paper I (and as in PGBYH), except for Fe^{+11} (see below). For the EA contribution we kept only the *D* term in equations (3) for simplicity (as in Paper I). The EA contribution was accurately enough reproduced with this simplified formula. When no measurements exist we adopted the new theoretical computations presented in PGBYH for the EA contribution. For Fe^{+9} we also adopted the theoretical estimates rather than the measured cross sections (dominated by ionization from metastable levels of excited ions in the beam, PGBYH). For Fe^{+11} (see Fig. 5) we slightly modified the parameters corresponding to DI ionization from the 3*p* shell to better fit the cross section below the EA threshold. The *D* parameter for the EA contribution was obtained by fitting the data above the EA threshold. The cross sections proposed in Paper I for Fe^{+13} are in good agreement with the measurements (see Fig. 6) and we kept the parameters proposed in Paper I.

The new rate coefficients obtained differ by less than 15% (usually 5%) from the ones computed from Paper I. The differences are essentially due to the EA contribution (neglected in Paper I for Fe^{+8} and Fe^{+9} and slightly overestimated for Fe^{+10}–Fe^{+12}).

Fe^{+15} (*configuration* $2s^22p^63s$).—The EA process was expected to be a major contribution in Fe^{+15} ionization (Cowan & Mann 1979; Sampson 1982). The results of Sampson (1982) we adopted in Paper I for this process, do not significantly differ from the new distorted wave calculations of Griffin et al. (1987). In Paper I we also included the contribution of the resonant-excitation double autoionization (REDA) as computed by LaGattuta & Hahn (1981)[3], which increases the rate coefficients by 10%–30% in the temperature range 6.3×10^5–5×10^6 K. Cross sections around the expected onset of the EA were measured by Gregory et al. (1987). The measurements clearly confirm the importance of the EA process. On the other hand, it is not clear if the REDA process further contributes or not to the cross sections (Gregory et al. 1987; Griffin et al. 1987). Though some of the expected enhancement (in particular around 750–780 eV) are lacking in the data, one notes that the cross sections computed with and without contribution

[2] Note that this is not the case for other iron ions of the same configurations ($3s^23p^63d^n$, $n < 6$): most of the 3*p* direct ionization contributes to the single ionization (PGBYH).

[3] We used the cross sections averaged over 20 eV energy bins.

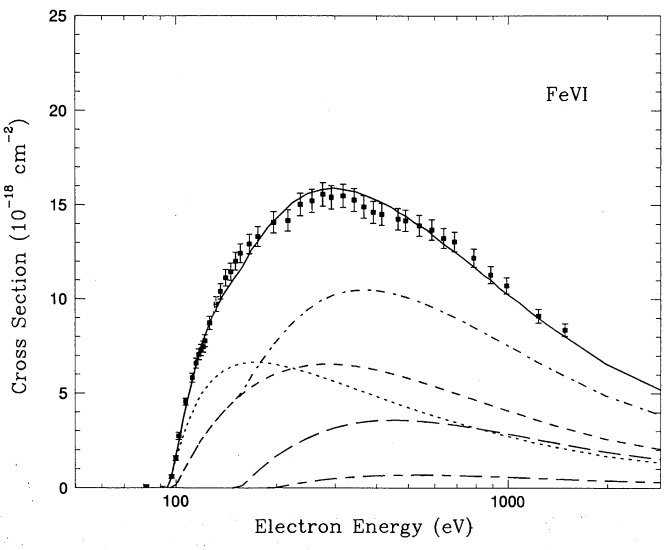

FIG. 3

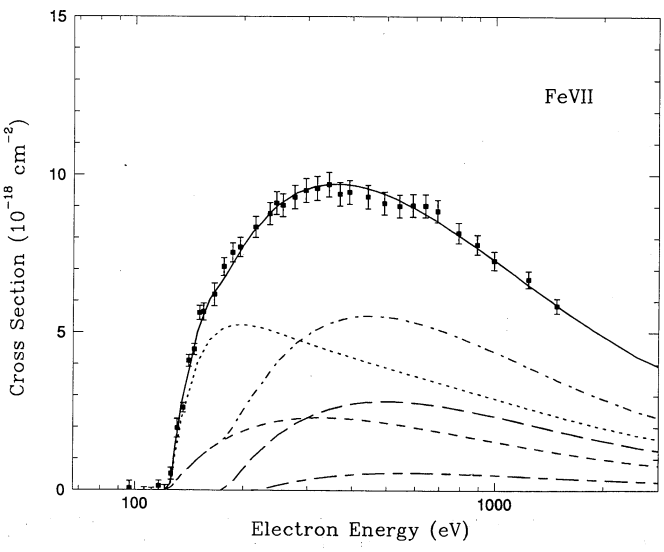

FIG. 4

FIG. 3.—Same as Fig. 1 for Fe^{+5}. Data points are from Gregory et al. (1986). *Dotted curve*: contribution of excitation autoionization. *Dot-dashed curve*: contribution of total direct ionization. *Short dashed curve*: contribution of direct ionization from 3*d* subshell. *Long dashed curve*: contribution of direct ionization from 3*p* subshell. *Long-short dashed curve*: contribution of direct ionization from 3*s* subshell.

FIG. 4.—Same as Fig. 3 for Fe^{+6}

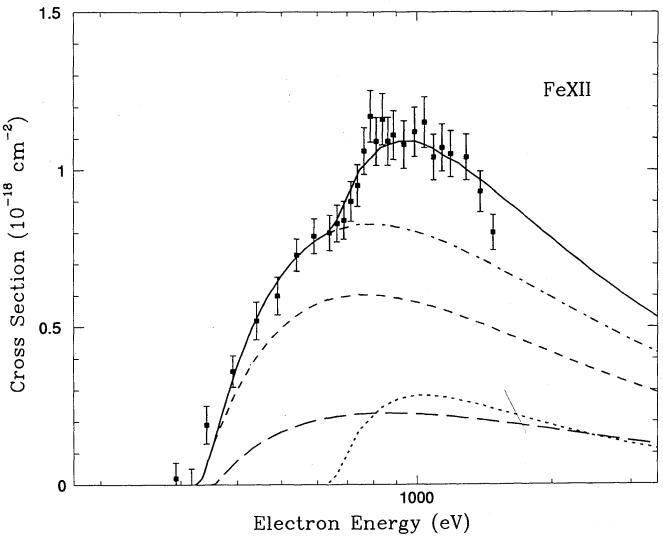

FIG. 5

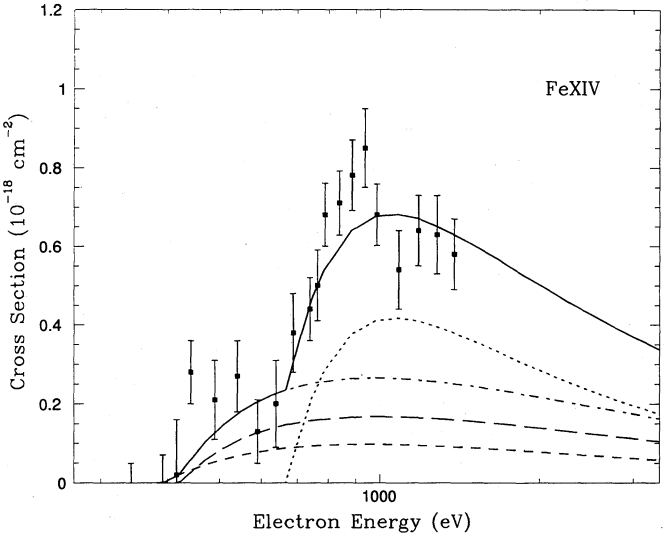

FIG. 6

FIG. 5.—Same as Fig. 1 for Fe^{+11}. Data points are from Gregory et al. (1987). *Dotted curve*: contribution of excitation autoionization. *Dot-dashed curve*: contribution of total direct ionization. *Short dashed curve*: contribution of direct ionization from 3*p* subshell. *Long dashed curve*: contribution of direct ionization from 3*s* subshell.

FIG. 6.—Same as Fig. 5 for Fe^{+13}

of the REDA process bracket the measured ones. In view of these results we decided to keep the rate coefficients proposed in Paper I.

Fe^{+16} *to* Fe^{+25}.—No measurements exist for these ions and we kept, as in Paper I and in PGBYH, the DWE computations of Younger (1982) for the DI process. Note, however, the misprint in the Table 2 of Younger (1982), which gives the coefficients allowing to compute the *A*, *B*, *C*, *D* parameters in formula (1): these coefficients correspond to *A*, *B*, *C*, *D* given in πa_o^2 ryd^2 and not in 10^{-14} cm^2 eV^2 as stated (compare the cross sections obtained with the results plotted in Figure 2 of Younger 1982 or the parameters obtained with those listed in Younger 1981b). Therefore the parameters listed in Table 1 of PGBYH for these ions must be multiplied by 1.626 as well as the corresponding ionization rate coefficients and Chebychev fitting parameters. The *A*, *B*, *C*, *D* parameters were correctly given in Paper I and are recalled in Table 1A. Finally there is a slight contribution (less than 5%) of the EA process for Fe^{+23} (Paper I based on computations by Sampson & Golden 1981). The results of Butler & Moores (1985), who compared in detail the cross sections obtained via different approximations, and of Rachafi, Defrance, & Brouillard (1987) clearly confirm these earlier estimates.

3. RADIATIVE RECOMBINATION RATES

The rate coefficient $\alpha_r(T)$ for radiative recombination of Fe^{+i+1} to Fe^{+i} at temperature T is written as

$$\alpha_r(T) = \alpha_g(T) + \sum_{n>n_g} \alpha_n(T) ,$$

where $\alpha_g(T)$ corresponds to radiative recombination to the ground state and $\alpha_n(T)$ to recombination to excited state of quantum number *n*. The quantity $\alpha_n(T)$ is the sum of the partial rate coefficients $\alpha_{nl}(T)$ corresponding to recombination to all the available subshells *nl* of shell *n* ($0 < l < n$ for $n > n_g$). The rate coefficients $\alpha_{nl}(T)$ can be computed from the partial cross sections σ_{nl} for photoionization of ion Fe^{+i} (subshell *nl*) using the Milne relation (Bates & Dalgarno 1962):

$$\alpha_{nl}(T) = 6.548 \times 10^{-17}(kT)^{3/2} x_{nl,i}^3 \exp(x_{nl,i}) \frac{g_i}{g_{i+1}} \int_1^\infty u^2 \sigma_{nl}(u) \exp(-u x_{nl,i}) du \qquad (5)$$

with

$$x_{nl,i} = \frac{\epsilon_{nl,i}}{kT} ,$$

where kT in eV, $\epsilon_{nl,i}$ is the binding energy of the electron in subshell *nl* of the recombined ion, *u* is the photon energy in units of $\epsilon_{nl,i}$, g_{i+1} and g_i are the statistical weight of recombining (ground state) and recombined (level *nl*) ions.

Till recently only cross sections corresponding to photoionization from ground states were available (Reilman & Manson 1979). Therefore the recombination rate coefficients for excited levels were computed using extrapolation along isonuclear sequence for the first excited levels and hydrogenic approximation afterwards (Woods et al. 1981; Paper I). The only exceptions concern recombination of H-like iron (Bely-Dubau et al. 1982) and He-like iron (Barfield 1979) for which more precise estimates were made (see also Paper I for a more detailed discussion of existing rate coefficients). Recently Clark et al. (1986) computed partial photoionization cross sections for subshells $1s \leq nl \leq 5g$ in He-like through Al-like isoelectronic sequences, using Hartree-Fock wave functions. We

reestimated the recombination rates of Fe^{+14} through Fe^{+25} from their photoionization cross sections via the Milne relation for levels up to $n = 5$. We used the hydrogenic approximation for levels with $n > 5$ (Seaton 1959).

It must be noted that the formulae given by Clark et al. (1986) for the photoionization cross sections are strictly valid only up to $u = 10$ (they are fits to the computations for $u < 10$). In particular, if extrapolated to higher energies, they do not ensure a correct asymptotic behavior: the cross sections decrease too slowly with increasing energy so that they usually do not obey the S_2 sum rule which requires that the integral $\int_1^\infty u^2\sigma_{nl}(u)du$ must not diverge (Rozsnyai & Jacobs 1988). However for our case of interest the exact asymptotic behavior of the cross sections is not important due to the rapidly decreasing exponential term in equation (5): the contribution of terms with $u > 10$ is less than 4% for $T/Z_{\rm eff}^2 < 2.0 \times 10^5$ K, where $Z_{\rm eff}^2$ is the effective charge of the recombining ion.

Another source of uncertainty is our use of the hydrogenic approximation for $n > 5$ levels. The hydrogenic approximation is more and more accurate as n increases, but it is also l dependent, the worst case being for $l = 0$. For instance the differences between the hydrogenic approximation and the "Clark et al." recombination rates for $n = 5$ and $l = 0$ range from typically 20% at $T/Z_{\rm eff}^2 = 10^3$ K to a factor as high as 3 at $T/Z_{\rm eff}^2 = 2 \times 10^4$ K. However the effect may be not drastic on the global rate because, on the other hand, the relative contribution of high n levels decreases with increasing temperature. An estimate of the error introduced by our approximation can be obtained by comparing, for instance, the rate coefficients obtained above to the rate coefficients computed using photoionization cross sections up to $n = 4$ only (instead of $n = 5$) and hydrogenic approximation afterwards ($n > 4$ instead of $n > 5$). The discrepancies are less than 4% (usually 2% or less) in the temperature range 1.25×10^3 K $< T/Z_{\rm eff}^2 < 2.0 \times 10^5$ K.

Differences between these new rate coefficients and previous estimates are not drastic; this essentially confirms the validity of Woods et al. (1981) approximations. In the temperature range, 1.25×10^3 K $< T/Z_{\rm eff}^2 < 2.0 \times 10^5$ K, for which Woods et al. (1981) provided a fit to the radiative recombination rate coefficients, the discrepancy is less than 20% for recombination of Fe^{+14} through Fe^{+22}. For Fe^{+23}, for which Arnaud & Rothenflug (1985) recomputed the recombination rate coefficients using Reilman & Manson photoionization cross sections (see Paper I, for a discussion of this point) it is less than 9% in the temperature range 10^4–10^8 K. Finally the discrepancies between our estimates and the detailed computations of Bely-Dubau et al. (1982) and Barfield (1979) for Fe^{+25} (5×10^6 K $< T < 10^8$ K) and Fe^{+24} (0.03 keV $< T <$ 3 keV) are less than 6%.

We fitted the rate coefficients obtained with an accuracy better than 5% in the temperature range 10^5 K–10^8 K, using the following formula

$$\alpha_r(T) = A\left[\frac{T}{10^4\ \mathrm{K}}\right]^{[-\alpha-\beta\ \log_{10}(T/10^4\ \mathrm{K})]} \mathrm{cm^3\ s^{-1}}\ . \tag{6}$$

The parameters A, α, and β are given in Table 2. Though more complicated than the power law used by previous authors (Aldrovandi & Péquignot 1973, 1976; Shull & Van Steenberg 1982a, b; Arnaud & Rothenflug 1985) this formula ensures a good fit of the rate coefficients over a much wider range in temperatures. This is especially important for computations concerning photoionized plasmas and recombining (cooling) plasmas where the temperature can be much lower than the temperature at which the ions have their maximum abundance in coronal ionization equilibrium situations.

4. DIELECTRONIC RECOMBINATION RATES

The Burgess (1965) General Formula and variants such as that proposed by Merts, Cowan, & Magee (1976) have been widely used to compute dielectronic recombination rates. A limitation of the General Formula is its intended use only near the peak temperature of an ion's abundance in collisional ionization equilibrium. In photoionized plasmas the General Formula may underestimate the dielectronic recombination rate by a large factor (Storey 1981; Nussbaumer & Storey 1983).

A second limitation was pointed out by Jacobs et al. (1977) In some cases the doubly excited levels formed in the first step of the dielectronic recombination process can Auger ionize not only the ground level (as assumed in the General Formula), but to other levels as well. Jacobs et al. (1977) found drastically reduced recombination rates by way of core electron transitions involving a change in principal quantum numbers. The Jacobs et al. calculations tend to overestimate the effect for highly charged ions,

TABLE 2

RADIATIVE RECOMBINATION COEFFICIENTS[a]

Ion	A ($\mathrm{cm^3\ s^{-1}}$)	α	β
Fe^{+14}.....	1.46 (−10)	0.597	5.22 (−2)
Fe^{+15}.....	1.68 (−10)	0.602	5.07 (−2)
Fe^{+16}.....	1.91 (−10)	0.601	5.10 (−2)
Fe^{+17}.....	2.24 (−10)	0.579	5.49 (−2)
Fe^{+18}.....	2.59 (−10)	0.567	5.65 (−2)
Fe^{+19}.....	2.96 (−10)	0.557	5.79 (−2)
Fe^{+20}.....	3.16 (−10)	0.534	6.02 (−2)
Fe^{+21}.....	3.49 (−10)	0.521	6.22 (−2)
Fe^{+22}.....	3.91 (−10)	0.523	6.15 (−2)
Fe^{+23}.....	4.33 (−10)	0.531	5.77 (−2)
Fe^{+24}.....	4.77 (−10)	0.537	5.49 (−2)
Fe^{+25}.....	5.84 (−10)	0.546	4.02 (−2)

[a] 1.46 (−10) denotes 1.46×10^{-10}.

TABLE 3

DIELECTRONIC RECOMBINATION COEFFICIENTS[a]

ION	E (eV)				c (cm^3 s^{-1} K$^{1.5}$)			
	E_1	E_2	E_3	E_4	c_1	c_2	c_3	c_4
Fe^{+1}	5.12 (0)	1.29 (1)	0	0	2.20 (−4)	1.00 (−4)	0	0
Fe^{+2}	1.67 (1)	3.14 (1)	0	0	2.30 (−3)	2.70 (−3)	0	0
Fe^{+3}	2.86 (1)	5.21 (1)	0	0	1.50 (−2)	4.70 (−3)	0	0
Fe^{+4}	3.73 (1)	6.74 (1)	0	0	3.80 (−2)	1.60 (−2)	0	0
Fe^{+5}	5.42 (1)	1.00 (2)	0	0	8.00 (−2)	2.40 (−2)	0	0
Fe^{+6}	4.55 (1)	3.60 (2)	0	0	9.20 (−2)	4.10 (−2)	0	0
Fe^{+7}	6.67 (1)	1.23 (2)	0	0	1.60 (−1)	3.60 (−2)	0	0
Fe^{+8}	6.61 (1)	1.29 (2)	0	0	1.80 (−1)	7.00 (−2)	0	0
Fe^{+9}	2.16 (1)	1.36 (2)	0	0	1.40 (−1)	2.60 (−1)	0	0
Fe^{+10}	2.22 (1)	1.44 (2)	0	0	1.00 (−1)	2.80 (−1)	0	0
Fe^{+11}	5.96 (1)	3.62 (2)	0	0	2.25 (−1)	2.31 (−1)	0	0
Fe^{+12}	7.50 (1)	2.05 (2)	0	0	2.40 (−1)	1.70 (−1)	0	0
Fe^{+13}	3.63 (1)	1.93 (2)	0	0	2.60 (−1)	1.60 (−1)	0	0
Fe^{+14}	3.94 (1)	1.98 (2)	0	0	1.90 (−1)	9.00 (−2)	0	0
Fe^{+15}	2.46 (1)	2.48 (2)	5.60 (2)	0	1.20 (−1)	1.20 (−1)	6.00 (−1)	0
Fe^{+16}	5.60 (2)	0	0	0	1.23 (0)	0	0	0
Fe^{+17}	2.25 (1)	1.17 (2)	3.41 (2)	6.83 (2)	2.53 (−3)	3.36 (−2)	1.81 (−1)	1.92 (0)
Fe^{+18}	1.62 (1)	9.60 (1)	3.30 (2)	7.29 (2)	5.67 (−3)	7.82 (−2)	3.18 (−2)	1.26 (0)
Fe^{+19}	2.37 (1)	8.51 (1)	3.29 (2)	7.87 (2)	1.60 (−2)	7.17 (−2)	9.06 (−2)	7.39 (−1)
Fe^{+20}	1.32 (1)	6.66 (1)	2.97 (2)	7.14 (2)	1.85 (−2)	9.53 (−2)	7.90 (−2)	1.23 (0)
Fe^{+21}	3.91 (1)	8.03 (1)	3.92 (2)	9.19 (2)	9.20 (−4)	1.29 (−1)	1.92 (−1)	9.12 (−1)
Fe^{+22}	7.32 (1)	3.16 (2)	8.77 (2)	0	1.31 (−1)	8.49 (−2)	6.13 (−1)	0
Fe^{+23}	1.00 (−1)	3.62 (1)	3.06 (2)	9.28 (2)	1.10 (−2)	4.88 (−2)	8.01 (−2)	5.29 (−1)
Fe^{+24}	4.625 (3)	6.00 (3)	0	0	2.56 (−1)	4.52 (−1)	0	0
Fe^{+25}	5.30 (3)	0	0	0	4.30 (−1)	0	0	0

[a] 1.00 (−1) denotes 1×10^{-1}.

however, because highly charged ions tend to recombine by way of relatively low-lying states which are energetically incapable of Auger ionizing to states other than the ground level (Beigman, Vainstein, & Chichkov 1981; Smith et al. 1985; Badnell 1986).

Since the works of Jacobs et al. (1977), there has been no comprehensive set of dielectronic recombination rate coefficients available, though detailed calculations have been made for many isoelectronic sequences. We have attempted to choose the most reliable rate coefficients, and we have fit them with the formula:

$$\alpha_{di}(T) = T^{-3/2} \sum c_i e^{-E_i/kT} \text{ cm}^3 \text{ s}^{-1} , \quad (7)$$

where T is in kelvin, kT and E_i are in eV, and c_i is in cm^3 s^{-1} K$^{1.5}$. The parameters c_i and E_i are given in Table 3.

The Burgess formula corresponds to a specification of c_i and E_i for each permitted transition of an ion. By adding terms with lower E_i, one can reproduce the low-temperature behavior which the Burgess formula fails to predict accurately. The fits generally reproduce the rate coefficients they are based upon to about 2%, which is far better than the likely accuracy of any of the computations. The following paragraphs discuss the rates chosen and compare with those employed by Arnaud & Rothenflug (1985) and the Shull & Van Steenberg (1982a) fits to and extension of Jacobs et al. (1977)[4].

Fe^{+25}.—We adopt the rates computed by Karim & Bhalla (1988), which are based on detailed calculations of the Auger and radiative transition probabilities of the individual resonances. These rates are about 35% below those given by Shull & Van Steenberg (1982a) and 15% above those used by Arnaud & Rothenflug (1985).

Fe^{+24}.—The rates computed by Chen (1986b) were used. These agree well with other theoretical calculations (Younger 1983b; Nasser & Hahn 1983). They are 22% lower than those of Shull & Van Steenberg (1982a) near 1 keV and 20% above those used by Arnaud & Rothenflug (1985).

Fe^{+23}.—The available calculations (Summers 1974; Jacobs et al. 1977; Zhdanov 1982; McLaughlin & Hahn 1984; Roszman 1987a; Romanik 1988) agree quite well for dielectronic recombination by way of the $2s$–$2p$ transition which dominates near 10^6 K, but they scatter over a factor of 4 at temperatures near 10^7 K where the ion is found in collisional equilibrium and where $2s$–$3p$ transitions dominate (see Fig. 7). We adopt the Romanik rates, which agree quite well with McLaughlin & Hahn (1984). These rates are 3 times larger than those of Shull & Van Steenberg (1982a) near a temperature of 1 keV.

Fe^{+22}.—Detailed calculations by McLaughlin, Lagattuta, & Hahn (1987), Badnell (1986), and Romanik (1988) are available. We adopt Badnell's calculations, which cover an extensive temperature grid and employ a detailed atomic model. Near 1 keV the rate is 2.48 times larger than that given by Shull & Van Steenberg (1982a, b).

Fe^{+21}.—Calculations by Badnell (1986) and Roszman (1990a) differ by about 60% at high temperatures, and the discrepancy is worse below 10^6 K. Ramadan & Hahn (1989) give rates at low temperatures closer to those of Badnell (1986). We adopt the Badnell's rates, which are 38% larger than Shull & Van Steenberg (1982a) at $T = 1$ keV.

[4] Arnaud & Rothenflug (1985) and Shull & Van Steenberg (1982a) adopted the same dielectronic recombination rates except for H- and He-like iron. They used the Jacobs et al. (1977) computations for Fe^{+8} through Fe^{+23} and the computations of Woods et al. (1981), based on the Burgess general formula for Fe^{+1} through Fe^{+7}.

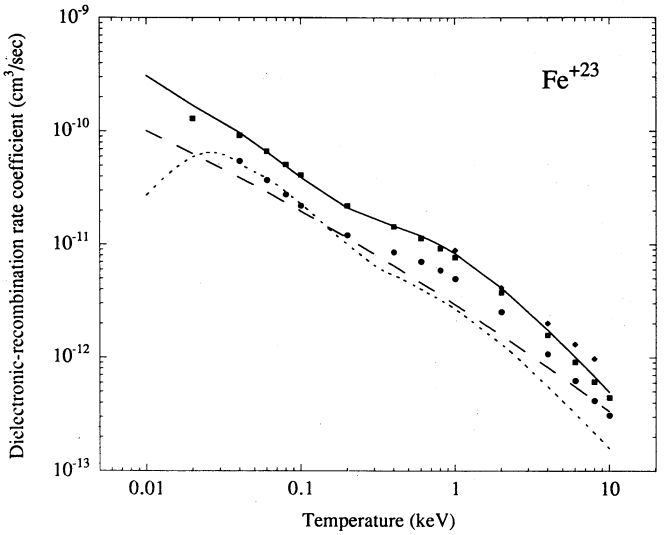

FIG. 7

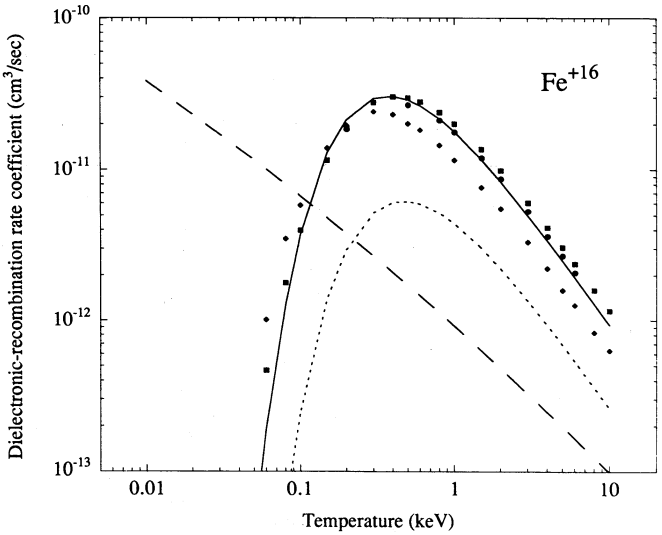

FIG. 8

FIG. 7.—Dielectronic recombination rate coefficients of Fe^{+23} vs. temperature. *Dotted curve*: rates from Jacobs et al. (1977), adopted by Shull & Van Steenberg (1982a) and Arnaud & Rothenflug (1985). *Diamonds*: computations of McLaughlin & Hahn (1984); *squares*: Romanik (1988); *circles*: Roszman (1987a). The full curve is the adopted rate coefficients (using eq. [6], the parameters are given in Table 3). For comparison we also plotted the radiative recombination rate coefficients vs. temperature (present work, *dashed curve*).

FIG. 8.—Same as Fig. 7 for Fe^{+16}. *Diamonds*: computations of Hahn (1989); *squares*: Romanik (1988); *circles*: Chen (1986b).

Fe^{+18}–Fe^{+20}.—Roszman's calculations (1987c, 1990a, b) are the only calculations available since those of Jacobs et al. (1977). They are smaller than those used by Arnaud & Rothenflug (1985) by 20%–50%.

Fe^{+17}.—Rates for this ion were computed by Roszman (1987b), Chen (1988), and Dasgupta & Whitney (1990). The latter two agree fairly well at low temperatures, while Roszman's rates agree better with Chen's at high temperatures. We adopt the Dasgupta & Whitney rates, which exceed Chen's by 34% at $T = 1$ keV. They are four times larger than the Shull & Van Steenberg (1982a) rates at temperatures where the ion is found in collisional equilibrium.

Fe^{+16}.—The neon-like ion has been studied by Beigman et al. (1981), Hahn (1989), Smith et al. (1985), Chen (1986b), and Romanik (1988). We adopt the Smith et al. rate scaled up by 40% to agree with the Chen and Romanik values (see Fig. 8). These rates are larger than the Jacobs et al. (1977) rates used by Shull & Van Steenberg (1982a) by a factor of 4.

Fe^{+12}–Fe^{+15}.—The fits to the Jacobs et al. (1977) rates given in Shull & Van Steenberg (1982a) were used with modifications to the high-temperature behavior where inner shell transitions of the form $2p$–$3d$ become important (Zhdanov 1982; Dube & LaGatutta 1987; Dube, Rosoanaivo, & Hahn 1985).

Fe^{+11}.—Rates from Hahn (1989), which are about 35% below those of Shull & Van Steenberg (1982a), are used.

Fe^{+9}, Fe^{+10}.—The high-temperature behavior of the Shull & Van Steenberg rates was modified to match the rates of Hahn (1989).

Fe^{+8}.—There is a factor of 3 discrepancy among the Burgess formula, the Hahn (1989) rate and the Jacobs et al. (1977) rates used by Shull & Van Steenberg (1982a). A calculation based on the Jacobs et al. (1977) formalism with the behavior of the partial wave collision strengths estimated from Fawcett & Mason (1991) supports the Hahn rate. We use the Burgess formula scaled down to match Hahn's rates (see Fig. 9).

Fe^{+1}–Fe^{+5}, Fe^{+7}.—The Shull & Van Steenberg (1982a) rates have been scaled to agree with those given by Hahn (1989). Hahn gives rates at only two temperatures, and these are generally above the temperatures where the ions occur in collisional ionization equilibrium. The Fe^{+1} and Fe^{+2} rates are drastically lower than those of Shull & Van Steenberg. Fortunately, in many astrophysical settings charge transfer with hydrogen will dominate the recombination rates of Fe^{+2} and Fe^{+3} (Neufeldt & Dalgarno 1987).

Fe^{+6}.—Rates from Hahn (1989) were adopted. They are somewhat lower than those of Shull & Van Steenberg (1982) at the temperatures where Fe^{+6} peaks, and they are much lower at higher temperatures.

5. IONIZATION EQUILIBRIA AND CONCLUSION

5.1. *Ionization Equilibria*

The ionization equilibria obtained in the framework of this study are tabulated along in Table 4 in the usual form of $-\log_{10} X_i$ versus $\log_{10} T$ where X_i is the ionic fraction and T is the temperature in Kelvin. In these calculations we assumed coronal equilibrium where three-body recombination and photoabsorption are negligible (low-density case). In this case the steady state ionic fractions do not depend on the electron density. We also give in Figure 10 the variation with temperature of the mean electric charge, together with the temperatures $T_{i,\max}$ at which the ionic fraction of each ion Fe^{+i} reaches its maximum. At $T_{i,\max}$ the mean charge is very close to $+i$: the ionic fractions are sharply peaked functions of the temperature and at $T_{i,\max}$ only the adjacent ions Fe^{+i+1} and Fe^{+i-1} have non-negligible abundances as compared to Fe^{+i}.

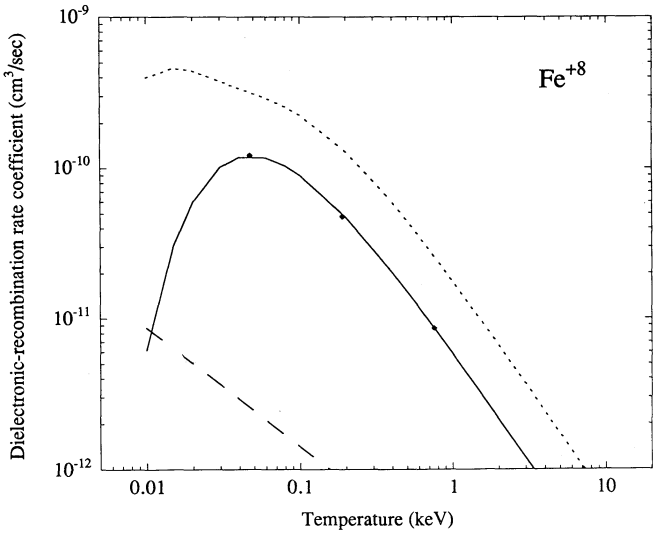

FIG. 9

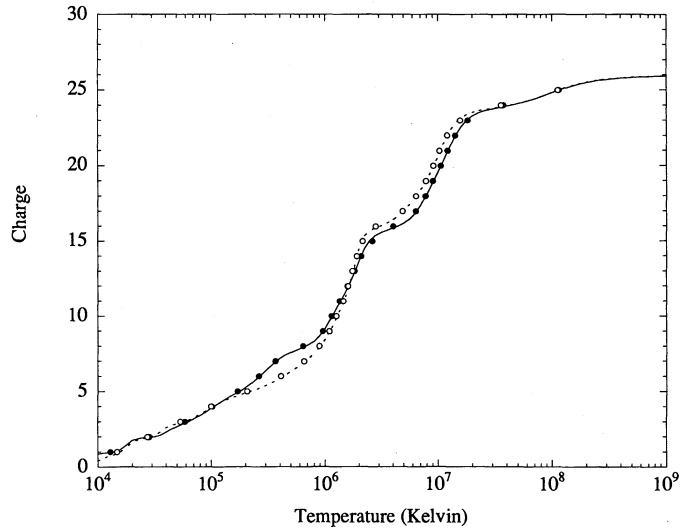

FIG. 10

FIG. 9.—Same as Fig. 7 for Fe^{+8}. *Diamonds*: computations of Hahn (1989).

FIG. 10.—Curves correspond to the mean electric charge vs. temperature. *Plain curve*: present work; *dashed curve*: from Arnaud & Rothenflug (1985). Each point corresponds to a given ion Fe^{+i}: the abscissa is the temperature at which its ionic fraction is maximum, the ordinate is the charge *i*. *Filled circles*: present work; *open circles*: from Arnaud & Rothenflug (1985).

For comparison we also displayed on Figure 10 the results of Arnaud & Rothenflug (1985). In our work iron is clearly more ionized at low temperature ($2 \times 10^5 < T < 10^6$ K), whereas it is the opposite at high temperature ($2 \times 10^6 < T < 1.5 \times 10^7$ K).

Our ionic fractions for Fe^{+5}–Fe^{+9} peaked at significantly lower temperatures (by 0.1–0.2 in log T) than those of Arnaud & Rothenflug (1985) or equivalently between 2×10^5 and 10^6 K where these ions are present the mean charge is higher. Note for instance that at log $(T) = 5.8$ the predominant ion is Fe^{+8} whereas it is Fe^{+7} in Arnaud & Rothenflug (1985). It is a direct consequence of our increase of the ionization rate (by a factor ~ 4 for Fe^{+5}–Fe^{+7}), together with an decrease (by about a factor of ~ 2) of the dielectronic recombination rate. To further illustrate this point we plotted on Figure 11 the ionic fractions versus temperature of Fe^{+7}–Fe^{+9}, for which the differences are the most drastic. Not only are the curves shifted to lower temperature, but their maximum values are different too. The maximum for Fe^{+8} is twice as high as the one given by Arnaud & Rothenflug and the Fe^{+8} curve now stands out above those of Fe^{+7} and Fe^{+9}. In the temperature range log $(T) = 5.6$–6, we have reduced the

TABLE 4

IONIZATION EQUILIBRIA

Log T(K)	+0	+1	+2	+3	+4	+5	+6	+7	+8
4.0	0.91	0.06	4.01	...	...	...	...	...	...
4.1	1.44	0.02	2.16	...	...	...	...	...	...
4.2	1.97	0.09	0.77	...	...	...	...	...	...
4.3	2.88	0.59	0.13	5.07	...	...	...	...	...
4.4	3.93	1.29	0.02	3.05	...	...	...	...	...
4.5	4.70	1.74	0.02	1.52	...	...	...	...	...
4.6	5.38	2.14	0.16	0.52	3.81	...	...	...	...
4.7	...	2.68	0.50	0.17	1.97	...	...	...	...
4.8	...	3.24	0.89	0.13	0.91	3.65	...	...	...
4.9	...	3.87	1.36	0.28	0.38	1.85	5.11	...	...
5.0	...	4.62	1.96	0.60	0.23	0.84	3.06	...	...
5.1	...	5.49	2.70	1.09	0.32	0.38	1.82	4.12	...
5.2	...	...	3.53	1.69	0.57	0.21	1.03	2.49	4.95
5.3	...	...	4.43	2.37	0.96	0.25	0.55	1.43	3.07
5.4	...	...	5.46	3.19	1.52	0.50	0.35	0.73	1.77
5.5	...	...	...	4.18	2.27	0.98	0.44	0.40	0.92
5.6	...	...	...	5.31	3.18	1.66	0.77	0.36	0.44
5.7	...	...	...	...	4.19	2.44	1.24	0.51	0.21
5.8	...	...	...	...	5.21	3.27	1.78	0.77	0.15
5.9	...	...	...	...	...	4.13	2.39	1.12	0.22
6.0	...	...	...	...	...	5.15	3.17	1.68	0.51
6.1	...	...	...	...	...	...	4.29	2.56	1.19
6.2	...	...	...	...	...	...	5.80	3.87	2.27
6.3	...	...	...	...	...	...	...	5.59	3.79
6.4	...	...	...	...	...	...	...	...	5.72
6.5	...	...	...	...	...	...	...	...	...

TABLE 4—*Continued*

log (T)	+ 9	+ 10	+ 11	+ 12	+ 13	+ 14	+ 15	+ 16	+ 17
5.0	...	...	...	...	...	...	...	...	...
5.1	...	...	...	...	...	...	...	...	...
5.2	...	...	...	...	...	...	...	...	...
5.3	...	...	...	...	...	...	...	...	...
5.4	5.94	...	...	...	...	...	...	...	...
5.5	4.02	...	...	...	...	...	...	...	...
5.6	2.66	5.21	...	...	...	...	...	...	...
5.7	1.72	3.48	5.57	...	...	...	...	...	...
5.8	1.05	2.17	3.59	5.35	...	...	...	...	...
5.9	0.62	1.21	2.06	3.22	5.10	...	...	...	...
6.0	0.49	0.64	1.01	1.66	2.93	4.44	...	...	...
6.1	0.81	0.57	0.53	0.75	1.50	2.42	3.63	4.28	...
6.2	1.58	1.01	0.61	0.45	0.75	1.16	1.82	2,10	5.34
6.3	2.81	1.96	1.25	0.75	0.66	0.62	0.83	0.83	3.28
6.4	4.50	3.39	2.41	1.61	1.17	0.74	0.57	0.35	2.17
6.5	...	4.91	3.68	2.62	1.88	1.11	0.62	0.20	1.51
6.6	...	...	4.92	3.61	2.59	1.52	0.76	0.16	1.05
6.7	...	...	...	4.58	3.31	1.97	0.98	0.20	0.73
6.8	...	...	...	5.60	4.10	2.52	1.32	0.37	0.58
6.9	...	...	...	...	5.10	3.31	1.91	0.80	0.73
7.0	...	...	...	...	...	4.41	2.83	1.56	1.24
7.1	...	...	...	...	...	5.84	4.09	2.66	2.11
7.2	...	...	...	...	...	...	5.65	4.07	3.30
7.3	...	...	...	...	...	...	...	5.60	4.63
7.4	...	...	...	...	...	...	...	...	5.95
7.5	...	...	...	...	...	...	...	...	...

log (T)	+ 18	+ 19	+ 20	+ 21	+ 22	+ 23	+ 24	+ 25	+ 26
6.0	...	...	...	...	...	...	...	...	...
6.1	...	...	...	...	...	...	...	...	...
6.2	...	...	...	...	...	...	...	...	...
6.3	...	...	...	...	...	...	...	...	...
6.4	4.20	...	...	...	...	...	...	...	...
6.5	2.95	4.63	...	...	...	...	...	...	...
6.6	2.00	3.13	4.73	...	...	...	...	...	...
6.7	1.28	1.95	3.07	4.37	5.92	...	...	...	...
6.8	0.79	1.08	1.79	2.67	3.74	5.06	...	...	...
6.9	0.63	0.59	0.96	1.46	2.13	3.05	3.84	...	...
7.0	0.88	0.56	0.61	0.80	1.13	1.69	2.10	...	...
7.1	1.52	0.94	0.73	0.64	0.67	0.92	1.02	4.92	...
7.2	2.49	1.67	1.22	0.88	0.65	0.63	0.49	3.54	...
7.3	3.62	2.59	1.91	1.35	0.87	0.61	0.25	2.62	5.60
7.4	4.74	3.52	2.64	1.86	1.17	0.69	0.15	1.96	4.35
7.5	5.82	4.41	3.34	2.38	1.49	0.80	0.11	1.46	3.35
7.6	...	5.28	4.02	2.88	1.81	0.93	0.11	1.06	2.55
7.7	...	...	4.70	3.38	2.14	1.09	0.14	0.76	1.90
7.8	...	...	5.37	3.90	2.50	1.28	0.21	0.54	1.39
7.9	...	...	...	4.44	2.88	1.51	0.32	0.41	1.01
8.0	...	...	...	5.01	3.31	1.79	0.48	0.34	0.71
8.1	...	...	...	5.60	3.76	2.10	0.67	0.34	0.50
8.2	...	...	...	...	4.23	2.44	0.88	0.38	0.35
8.3	...	...	...	...	4.70	2.78	1.11	0.44	0.25
8.4	...	...	...	...	5.17	3.13	1.35	0.53	0.18
8.5	...	...	...	...	5.64	3.47	1.58	0.63	0.13
8.6	...	...	...	...	...	3.81	1.81	0.73	0.10
8.7	...	...	...	...	...	4.14	2.03	0.83	0.07
8.8	...	...	...	...	...	4.46	2.24	0.94	0.06
8.9	...	...	...	...	...	4.77	2.45	1.04	0.04
9.0	...	...	...	...	...	5.07	2.65	1.14	0.03

recombination rate of Fe^{+8} by a factor 2.5 and increased the ionization rate of Fe^{+7} by a factor 6.9–3.7, thus drastically increasing the ratio Fe^{+8}/Fe^{+7}.

At high temperatures ($2 \times 10^6 < T < 1.5 \times 10^7$ K, species Fe^{+15}–Fe^{+23}) the shift toward higher temperatures is clearly due to our increase of the dielectronic rates (the ionization rates are essentially the same as in Arnaud & Rothenflug and the differences for the radiative rates are not drastic). The ionic fractions we obtained for Fe^{+16} and adjacent ions are dramatically changed (see Fig. 12). The ions peaked at higher temperatures but also the Fe^{+16} curve is less prominent and broader, whereas the maximum of the Fe^{+15} curve is twice as high. The ionization rate of the sodium-like Fe^{+15} is high while the recombination of the neon-like Fe^{+16} is very low. Therefore Fe^{+15} is never very abundant while Fe^{+16} can reach very large abundances and its curve stands out above those of adjacent ions (see Fig. 12 and the plateau around 4×10^6 K in Fig. 10). In increasing the recombination rate by a factor ~ 4

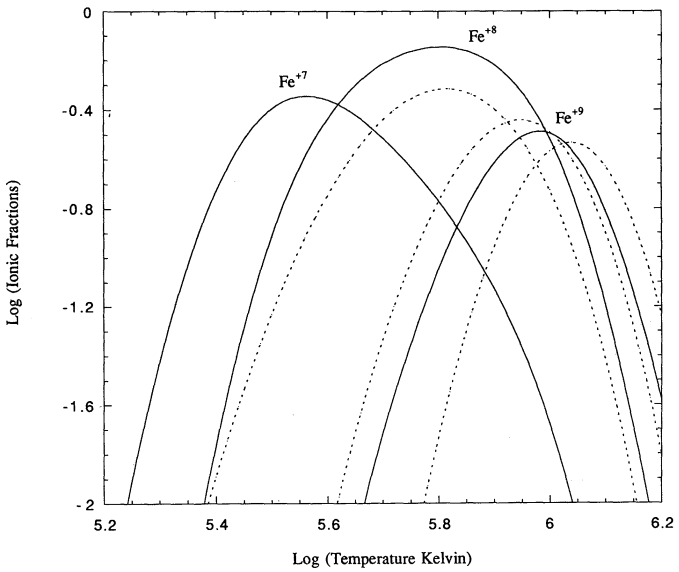

FIG. 11

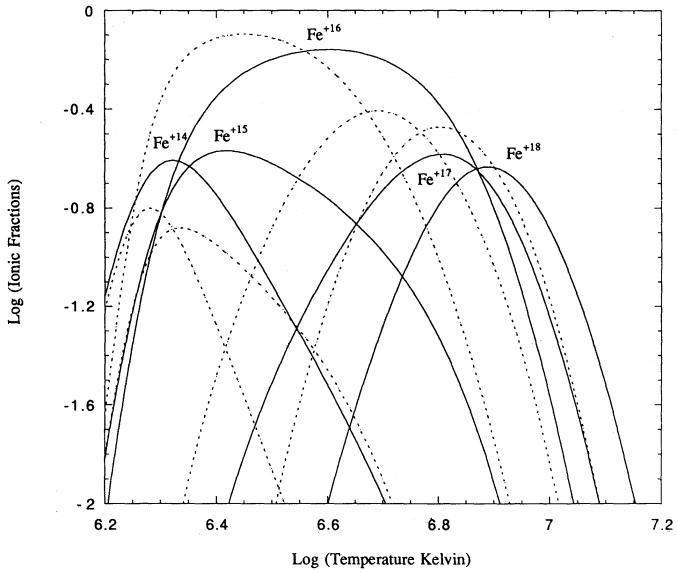

FIG. 12

FIG. 11.—Ionic fractions vs. temperature for Fe^{+7}, Fe^{+8}, and Fe^{+9}. *Plain curves*: present work; *dashes curves*: from Arnaud & Rothenflug (1985).
FIG. 12.—Same as Fig. 11 for Fe^{+14} through Fe^{+18}

we have significantly decreased this effect. Also Fe^{+15} is now abundant on a larger temperature range after its maximum, resulting also in the broadening of the Fe^{+16} curve observed before its maximum (see Fig. 12).

5.2. *Comparison with Measured Ionization Balance*

Many authors over the last decade have used the H- and He-like ion resonance lines and the satellite lines produced by lower ionization species to derive electron temperatures and relative abundances of iron ions in solar flares and in laboratory plasmas (see review by Doschek 1990). The results are compared with coronal equilibrium models to infer departures from ionization equilibrium or to suggest revised values for the equilibrium ionization (e.g., Doschek & Feldman 1987; Lemen et al. 1984; Tanaka 1986; Antonucci et al. 1987). Typical results are departures from equilibrium during a very short period at the onset of a flare and a general discrepancy between theoretical and empirical ion density ratios through the flare's duration. Tanaka (1986) finds a higher ratio $N(Fe^{+25})/N(Fe^{+24})$ than expected. Antonucci et al. (1987) find larger ratios of Fe^{+22} and Fe^{+23} to Fe^{+24} than predicted by most ionization balance calculations.

The comparison with empirical ionization balance determinations carries the danger that errors in measured line intensities or errors in the excitation, autoionization, or radiative transition probabilities of the lines employed will lead to erroneous conclusions, but most authors agree that the ionization balance is the most uncertain of the quantities entering the comparison. It is also probable that many temperatures contribute to the observed emission, and that the values of electron temperature and ion density ratio derived from spectra represent differently weighted averages over the temperature range (Raymond & Smith 1986). However, extensive calculations by Doschek & Feldman (1987) show that this averaging cannot account for the known discrepancies between theoretical and empirical ionization states.

Ion density ratios derived from *SOLFLEX*, *Hinotori*, and *SMM* all yield similar results. As shown in Antonucci et al. (1987), the Fe^{+23}/Fe^{+24} ratio is about 1.5 times larger at all temperatures than predicted by Arnaud & Rothenflug (1985), while the empirical Fe^{+22}/Fe^{+24} is larger than predicted by about a factor of 2.5. The Fe^{+25}/Fe^{+24} ratio derived by Tanaka (1986) is larger than predicted by roughly a factor of 3. The ionization balance calculations of this paper agree with those of Arnaud & Rothenflug (1985) for the Fe^{+23} and Fe^{+25} to Fe^{+24} ratios to within about 5% through the relevant temperature range. The new predictions for Fe^{+22}/Fe^{+24} are larger than those of Arnaud & Rothenflug by a factor of 2, however. The change results largely from the increased dielectronic recombination rate of Fe^{+23} compared with the Jacobs et al. (1977) rates used previously. Thus the new calculations do nothing to alleviate the problems with Fe^{+25} or Fe^{+23}, but they nearly remove the Fe^{+22} problem. Had we adopted the Roszman (1987a) dielectronic recombination rate for Fe^{+23}, the lower rate would somewhat improve the agreement of this ion with solar observations.

There are several possible explanations for the remaining discrepancies. Uncertainties in the measured line intensities or the excitation rates of the lines might cause errors on the empirical values of T_e or $N(Fe^{+23})/N(Fe^{+24})$. This seems to require errors on the order of 50%, which is implausibly large. Large uncertainties in the dielectronic recombination rates are ruled out as well, because the dielectronic recombination rates are derived from the same rates which go into the T_e determination and because the satellite lines in effect measure the dielectronic recombination rates. Thus if atomic rates are to blame, the radiative recombination rates of Fe^{+25} and Fe^{+24} or the collisional ionization rates of Fe^{+23} and Fe^{+24} are the only candidates. Our examination of the radiative recombination rates in § 3 above suggests that these cannot account for more than about 15% errors. Therefore, we conclude that if atomic rate uncertainties are to account for the discrepancy, they must reside mainly in the Fe^{+23} and Fe^{+24} collisional ionization rates. A decrease in the Fe^{+23} ionization rate by about a factor of 1.5 is not unthinkable, and in fact the Doyle

& Raymond (1981) ionization balance agrees fairly well with the empirical Fe^{+23}/Fe^{+24} ratio because of the lower ECIP ionization rate of Summers (1974). However, a factor of 3 increase in the Fe^{+24} ionization rate to match the Fe^{+25}/Fe^{+24} ratio seems much more difficult to accept.

It is also possible that the coronal ionization balance is simply inappropriate to the observed solar flares. Laboratory spectra show discrepancies much like those observed in solar flares, and the laboratory spectra are attributed to diffusion across the steep gradients in laboratory plasmas (e.g., the analysis of Ni by Bitter et al. 1991). This interpretation would require that the solar flare plasma has fine structure on scales of meters. Time-dependent ionization is another possibility, though it might require a flare to consist of many microscopic releases of energy to allow small volumes of gas to heat and cool over times shorter than the relevant ionization and recombination times (see Doschek 1990). Departures from Maxwellian electron velocity distributions provide a third possibility.

We thank T. Kato, K. Masai, and R. Rothenflug for fruitful discussions and their very useful comments on the manuscript. This work was supported by NASA grant NAGW-548 to the Smithsonian Astrophysical Observatory.

REFERENCES

Aldrovandi, S. M. V., & Péquignot, D. 1973, A&A, 25, 137
———. 1976, A&A, 47, 321
Antonucci, E., Dodero, M. A., Gabriel, A. H., Tanaka, K., & Dubau, J. 1987, A&A, 180, 263
Arnaud, M., & Rothenflug, R. 1985, A&AS, 60, 425 (Paper I)
Badnell, N. R. 1986, J. Phys. B, 19, 3827
Barfield, W. D. 1979, ApJ, 229, 856
Bates, D. R., & Dalgarno, A. 1962, in Atomic and Molecular Processes, ed. D. R. Bates (New York: Academic Press), 245
Beigman, I. L., Vainstein, L. A., & Chichkov, B. N. 1981, Soviet Phys. JETP, 53, 190
Bely-Dubau, F., Dubau, J., Faucher, P., & Gabriel, A. H. 1982, MNRAS, 198, 239
Bitter, M. 1991, Phys. Rev. A, 41, 1427
Burgess, A. 1965, ApJ, 141, 1588
Butler, K., & Moores, D. L. 1985, J. Phys. B, 18, 1247
Chen, M. H. 1986a, Phys. Rev. A, 33, 994
———. 1986b, Phys. Rev. A, 34, 1073
———. 1988, Phys. Rev. A, 38, 2332
Clark, R. E. H., Cowan, R. D., & Bobrowicz, F. W. 1986, Atomic Data and Nuclear Tables, 34, 415
Cowan, R. D., & Mann, J. B. 1979, ApJ, 232, 940
Dasgupta, A., & Whitney, K. G. 1990, Phys. Rev. A, 42, 2640
Doschek, G. A. 1990, ApJS, 73, 117
Doschek, G. A., & Feldman, U. 1987, ApJ, 313, 883
Doyle, J. G., & Raymond, J. C. 1981, MNRAS, 196, 907
Dube, M. P., & LaGatutta, K. J. 1987, J. Quant. Spectros. Rad. Transf., 38, 311
Dube, M. P., Rosoanaivo, R., & Hahn, Y. 1985, J. Quant. Spectros. Rad. Transf., 33, 13
Fawcett, B. C., & Mason, H. E. 1991, Atomic Data Nucl. Data, 47, 17
Golden, L. B., Clark, R. E. H., Goett, S. J., & Sampson, D. H. 1981, ApJS, 45, 603
Gregory, D. C., Meyer, F. W., Müller, A., & Defrance, P. 1986, Phys. Rev. A, 34, 3657
Gregory, D. C., Wang, L. J., Meyer, F. W., & Rinn, K. 1987, Phys. Rev. A, 35, 3256
Griffin, D. C., Pindzola, M. S., & Bottcher, C. 1987, Phys. Rev. A, 36, 3642
Hahn, Y. 1989, J. Quant. Spectros. Rad. Transf., 41, 315
Hahn, Y., Gau, J. N., Luddy, R., Dube, M., & Shkolnik, N. 1980, J. Quant. Spectros. Rad. Transf., 24, 505
Jacobs, V. L., Davis, J., Kepple, P. C., & Blaha, M. 1977, ApJ, 211, 605
Karim, K. R., & Bhalla, C. P. 1988, Phys. Rev. A, 37, 2599
LaGattuta, K. J., & Hahn, Y. 1981, Phys. Rev. A, 24, 2273
Lemen, J. R., Phillips, K. H. J., Cowan, R. D., Hata, J., & Grant, I. P. 1984, A&A, 135, 313
McGuire, E. J. 1977, Phys. Rev. A, 16, 62
McLaughlin, D. J., & Hahn, Y. 1984, Phys. Rev. A, 29, 712
McLaughlin, D. J., LaGatutta, K. J., & Hahn, Y. 1987, J. Quant. Spectros. Rad. Transf., 37, 47
Merts, A. L., Cowan, R. D., & Magee, N. H., Jr. 1976, Los Alamos Sci. Lab. Rep. LA-6220-MS
Mewe, R. 1972, A&A, 20, 215
Montague, R. G., Diserens, M. J., & Harrison, M. F. A., 1984, J. Phys. B, 17, 2085
Mueller, D. W., Morgan, T. J., Dunn, G. H., Gregory, D. C., & Crandall, D. H. 1985, Phys. Rev. A, 31, 2095
Nasser, I., & Hahn, Y. 1983, J. Quant. Spectros. Rad. Transf., 29, 1
Neufeldt, D., & Dalgarno, A. 1987, Phys. Rev. A, 35, 3142
Nussbaumer, H., & Storey, P. J. 1983, A&A, 126, 75
Pindzola, M. S., Griffin, D. C., & Bottcher, C. 1986, Phys. Rev. A, 34, 3668
Pindzola, M. S., Griffin, D. C., Bottcher, C., Younger, S. M., & Hunter, H. T. 1987, Nucl. Fusion, Special Suppl. 1987, 21 (PGBYH)
Rachafi, S., Defrance, P., & Brouillard, F. 1987, J. Phys. B, 20, L665
Ramadan, H. H., & Hahn, Y. 1989, Phys. Rev. A, 39, 3350
Raymond, J. C., & Smith, B. W. 1986, ApJ, 306, 762
Reilman, R., & Manson, S. T. 1979, ApJS, 40, 815
Romanik, C. J. 1988, ApJ, 330, 1022
Roszman, L. J. 1987a, Phys. Rev. A, 35, 2122
———. 1987b, Phys. Rev. A, 35, 2138
———. 1987c, Phys. Rev. A, 35, 3368
———. 1990a, private communication
———. 1990b, private communication
Rozsnyai, B. F., & Jacobs, V. L. 1988, ApJ, 327, 485
Sampson, D. H., & Golden, L. B. 1981, J. Phys. B, 14, 903
Sampson, D. H. 1982, J. Phys. B, 15, 2087
Seaton, M. J. 1959, MNRAS, 119, 81
Shull, J. M., & Van Steenberg, M. 1982a, ApJS, 48, 95
———. 1982b, ApJS, 49, 351
Smith, B. W., Raymond, J. C., Mann, J., & Cowan, R. D. 1985, ApJ, 298, 898
Storey, P. J. 1981, MNRAS, 195, 27P
Summers, H. P. 1974, Culham Lab. Internal Memo IM-367
Tanaka, K. 1986, PASJ, 38, 225
Woods, D. T., Shull, J. M., & Sarazin, C. L. 1981, ApJ, 249, 399
Younger, S. M. 1981a, J. Quant. Spectros. Rad. Transf., 24, 1272
———. 1981b, J. Quant. Spectros. Rad. Transf., 26, 329
———. 1982, J. Quant. Spectros. Rad. Transf., 27, 541
———. 1983a, J. Quant. Spectros. Rad. Transf., 29, 61
———. 1983b, J. Quant. Spectros. Rad. Transf., 29, 67
Zhdanov, V. P. 1982, J. Phys. B, 15, L537